JOURNAL OF APPLIED ELECTROCHEMISTRY 25 (1995) 212–218

Surface treatment for mitigation of hydrogen absorption and penetration into AISI 4340 steel and Inconel 718 alloy

G. ZHENG, B. N. POPOV, R. E. WHITE

Department of Chemical Engineering, University of South Carolina, Columbia, SC, 29208, USA

Received 18 August 1983; revised 15 July 1994

It is shown that the underpotential deposition of zinc on AISI 4340 steel and Inconel 718 alloys inhibits the hydrogen evolution reaction and the degree of hydrogen ingress. In the presence of monolayer coverage of zinc on the substrate surfaces, the hydrogen evolution current densities are reduced 46% and 68% compared with the values obtained on bare AISI 4340 steel and Inconel 718 alloy, respectively. As a consequence, the underpotential deposition of zinc on AISI 4340 steel and Inconel 718 alloy membrane reduces the steady state hydrogen permeation current density by 51% and 40%, respectively.

List of symbols

C_s	surface hydrogen concentration (mol cm^{-3})
D	hydrogen diffusion coefficient (cm^2 s^{-1})
E	potential (V)
E_{pdep}	predeposition potential (V)
F	Faraday constant (96 500 C mol^{-1})
i	current density (A cm^{-2})
i_a	HER current density in the absence of predeposition of zinc (A cm^{-2})
i_0	exchange current density (A cm^{-2})
i_p	HER current density in the presence of predeposition of zinc (A cm^{-2})
j_t	transition hydrogen permeation current density (A cm^{-2})
j_o	initial hydrogen permeation current density (A cm^{-2})
j_∞	steady state hydrogen permeation current density (A cm^{-2})
k''	thickness dependent absorption-adsorption constant (mol cm^{-3})
L	membrane thickness (cm)
Q_{max}	maximum charge required for one complete layer of atoms on a surface (C cm^{-2})
t	time (s)

Greek symbols

α_c	cathodic transfer coefficient, dimensionless
θ_H	hydrogen surface coverage, dimensionless
θ_{Zn}	zinc surface coverage, dimensionless
ϕ	work function (eV)
$\tau = tD/L^2$	(dimensionless time)

1. Introduction

Hydrogen embrittlement occurs as a result of hydrogen absorption on the metal surface followed by diffusion into the crystalline lattice of the substrate [1, 2]. Regardless of the various methods to decrease hydrogen embrittlement [3, 4], it is difficult to reduce the hydrogen penetration rate onto the alloy substrate to a level which provides the elimination of hydrogenation cracking hazards. It is known that if the hydrogen permeation rate through a metal membrane is described by Fick's laws of diffusion, and with a zero surface concentration of hydrogen at the anodic side, then the steady state hydrogen permeation current density through the membrane will be [5]

$$j_\infty = \frac{FDC_s}{L} \quad (1)$$

where j_∞ is the steady state hydrogen permeation current density, F the Faraday constant, D the hydrogen diffusion coefficient through the membrane, C_s the concentration of hydrogen in the membrane at the cathodic side, and L the thickness of the membrane. Further, assuming the surface-to-bulk (adsorption-absorption) reaction is in equilibrium, then Equation 1 will become

$$j_\infty = \frac{FDk''\theta_H}{L} \quad (2)$$

where k'' is the thickness dependent absorption-adsorption constant, and θ_H the hydrogen surface coverage. From Equation 2 it can be seen that for the same metal membranes the hydrogen permeation rate may be inhibited by either reducing the hydrogen surface coverage θ_H or by decreasing the absorption-adsorption constant k''.

0021-891X

Underpotential deposition (UPD) occurs at potentials more noble than the reversible Nernst potential. It occurs when ions of a lower work function metal are in contact with a higher work function substrate [6–8]. The underpotential shift ΔE in V is proportional to the difference in work functions $\Delta\phi$ in eV of both metals:

$$\Delta E = 0.5\Delta\phi \quad (3)$$

Drazic and Vorkapic [9] established that the presence of metal ions (Cd^{2+}, Mn^{+} and Zn^{2+}) more electronegative than the cathodic potential for the hydrogen evolution reaction on iron in a 0.25 M H_2SO_4 solution, inhibits the hydrogen evolution reaction and corrosion of iron. This effect has been explained as the underpotential deposition of the adatoms of these metals on iron. By investigating the mechanism of electrochemical reduction of zinc, Despic and Pavlovic [10] found that in slightly acidic sulphate electrolytes, zinc ions are underpotential deposited on gold and platinum substrates. Rashkov *et al.* [11] reported that UPD zinc submonolayer inhibited the discharge of hydrogen ions and reduced the amount of hydrogen ingress into iron substrate. By comparing cyclic voltammetry results with data derived from the Devanathan–Stachurski method (under identical conditions), the UPD of zinc, bismuth and lead on AISI 4340 steel and Monel K 500 reduced the amount of both atomic hydrogen adsorbed and the degree of hydrogen ingress in the alloy [12–16].

The aim of this work is to estimate the effectiveness of UPD of zinc on the reduction of the hydrogen evolution rate and the degree of hydrogen ingress into AISI 4340 steel and Inconel 718 alloy. The sharp reduction in corrosion rate was expected due to the kinetic limitations of the hydrogen discharge reaction on the deposited monolayers. As a consequence, one can expect a decrease of the hydrogen surface coverage to decrease the hydrogen penetration rate into the alloy.

2. Experimental details

The Tafel and linear sweep voltammetry were used to investigate the possibility of the underpotential deposition of zinc on AISI 4340 steel and Inconel 718 alloy and to determine the diagnostic criteria for the identification of the mechanism of hydrogen discharge in the presence and absence of underpotential deposited zinc as well as to determine the experimental UPD conditions. The Devanathan–Stachurski permeation technique [17] was used to investigate the rate of hydrogen permeation through AISI 4340 steel and Inconel 718 alloy membrane.

The electrochemical cell employed for these studies was a conventional three-compartment design with contact between the working electrode compartment and the reference electrode via a Luggin probe. The polarization experiments were carried out using AISI 4340 steel and Inconel 718 alloy electrode with a geometric area of 0.5 cm^2.

Using the Devanathan–Stachurski permeation technique, the rate of hydrogen permeation through AISI 4340 steel or Inconel 718 was measured continuously as a function of time. The permeation rate through a thin membrane of the steel was measured by setting the potential on the 'diffusion side' of the membrane (the side from which the hydrogen emerges) at a value which corresponds to a practically zero concentration of absorbed atomic hydrogen on the surface [17]. These experiments were carried out in a system with two working compartments, separated by a bipolar AISI 4340 steel or Inconel 718 alloy membrane. The membrane on the cathodic side of the cell was polarized potentiostatically, creating conditions for underpotential deposition and hydrogen evolution. In the anodic compartment of the cell, the membrane was polarized potentiostatically at −0.3 V vs the Hg/HgO reference electrode and the amount of oxidized atomic hydrogen was monitored continuously using a chart recorder. Prior to the permeation experiment, the AISI 4340 steel membrane was mechanically polished with 0.3 μm high purity alumina powder to a mirror finish, cleaned in an ultrasonic cleaning bath and saturated with hydrogen in 0.1 N H_2SO_4 by maintaining for 10 h (48 h for Inconel 718 alloy membrane) at a cathodic current density of 10 mA cm^{-2}. Then, the steel membrane was etched for 20 s in a solution containing methyl alcohol and 1% H_2SO_4 (in 1 : 1 sulfuric acid and nitric acid solution for Inconel 718 alloy), rinsed with deionized water, dried in air and fitted into the permeation cell. To avoid a possible passivation or dissolution, the anodic side of the membrane was coated with a thin layer (0.15–0.20 μm) of palladium. The deposition was carried out in an electrolyte containing 2×10^{-5} M $Na_2Pd(NO_2)_4$ using a current density of 100 μA cm^{-2} for 2 h. Then, the electrolyte was drained off, and the compartment was washed with deionized water and filled with the anodic solution. To keep the electrolyte impurities in the lowest possible level, the anodic solution (0.2 M NaOH), prior to introducing it in the compartment, was preelectrolysed for at least 24 h in a separate electrolytic cell. The anolyte was kept at −0.3 V vs the Hg/HgO reference electrode until the background current was reduced below 3 μA cm^{-2} (0.03 μA cm^{-2} for Inconel 718). Then, the cathodic compartment was filled with a supporting electrolyte and the experiments were carried out. Prepurified nitrogen was bubbled through both compartments in order to keep them free from oxygen contamination.

3. Results and discussion

3.1. *Cyclic voltammetry*

Linear sweep voltammetric curves obtained on AISI 4340 steel electrodes by using an electrolyte

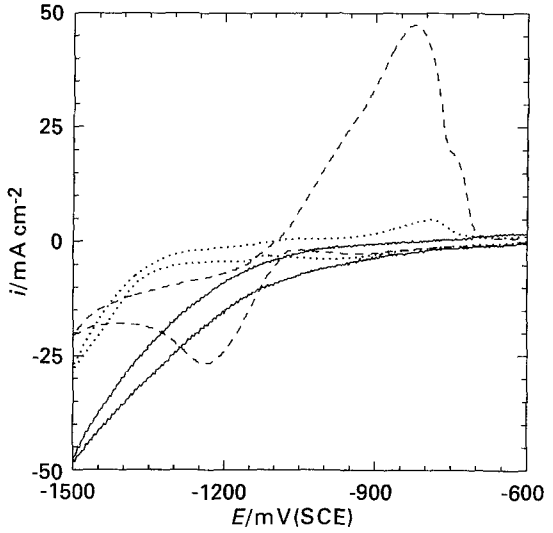

Fig. 1. Cyclic voltammetry curves obtained on AISI 4340 electrode by using an electrolyte containing 1 M Na_2SO_4, 0.4 M NaCl, 1 M H_3BO_3 (pH 4) for different concentrations of Zn^{2+}, and sweep rate 500 mV s^{-1}. Key: (——) without Zn^{2+}; (·····) 5×10^{-3} M Zn^{2+}; (– – –) 0.1 M Zn^{2+}.

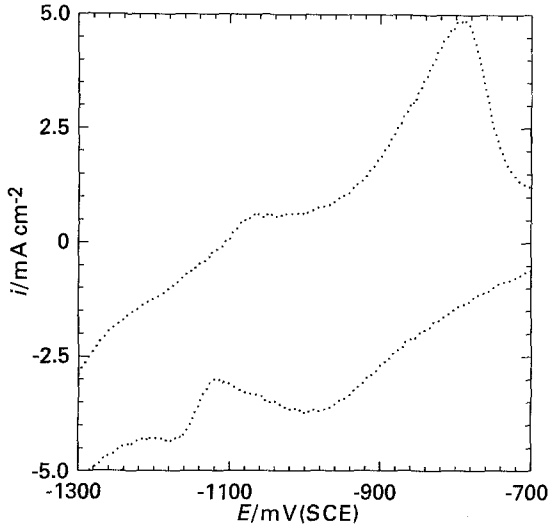

Fig. 2. Cyclic voltammetry curves obtained on AISI 4340 electrode by using an electrolyte containing 1 M Na_2SO_4, 0.4 M NaCl, 1 M H_3BO_3 (pH 4), Zn^{2+}. Concentrations 5×10^{-3} M and sweep rate 500 mV s^{-1}. Key: (·····) 5×10^{-3} M Zn^{2+}.

containing 1 M Na_2SO_4, 0.4 M NaCl, 1 M H_3BO_3 (pH 4) for different concentrations of zinc ions with a sweep rate of 500 mV s^{-1} are given in Fig. 1. In the presence of zinc ions in the electrolyte and starting the cathodic sweep from −600 mV vs SCE, two well defined peaks are observed in Fig. 1. The first peak occurs at −980 mV vs SCE (for zinc concentrations of 5×10^{-3} M) and is more noble than the corresponding Nernst potentials (−1070 mV vs SCE) of a zinc electrode. A second peak develops at −1170 mV vs SCE and corresponds to the bulk deposition of zinc deposition from the electrolyte. In Fig. 1, the underpotential shifts in the presence of 5×10^{-3} M and 0.1 M zinc ions are 290 mV and 190 mV, respectively. Using the work function values for iron and zinc [18] and Equation 3, the underpotential shift was calculated to be in the range of 180 to 310 mV which is consistent with our observed experimental values. On the anodic side in the presence of 5×10^{-3} M zinc ions, two stripping peaks are observed and correspond to the zinc dissolution and zinc desorption peak.

Since the underpotential deposition peak in the potentiodynamic curves given in Fig. 1 was not clearly visible, the voltammetric curve obtained for Zn^{2+} concentration of 5×10^{-3} M was enlarged and is presented in Fig. 2. The shape of the cathodic and anodic curve in Fig. 2 indicates that in the presence of 5×10^{-3} M zinc ions in the electrolyte at −980 mV vs SCE and at −790 mV vs SCE an adsorption–desorption process occurs on an AISI 4340 steel membrane with peak currents corresponding to the underpotential deposition and desorption of zinc. The large peak separation can be explained taking into account that the observed UPD is not a simple reversible process. A possibility exists of alloying between the UPD zinc and iron substrate. In this instance, the stripping wave for alloyed zinc might be shifted to more noble values. Such alloying effects between substrate and a UPD layer are well known for other systems such as Zn–Cu, Au–Ag, Cd–Sn, Pb–Au [6]. McBreen *et al.* [19, 20] reported alloying of the UPD zinc and silver substrate. The striping wave for alloyed zinc in this system was shifted at potential 1.0 V more anodic than underpotential stripping peak. According to Fig. 1, the zinc deposition peak increases as the zinc content in the electrolyte is increased. This phenomena is not observed for the process occurring at UPD region indicating that the zinc adsorption on AISI 4340 steel has reached an equilibrium value and does not depend on the amount of the dissolved zinc ions in the electrolyte. This statement appears to violate the Nernstian formulation of the UPD process. At fixed potential according to Nernstian formulation of UPD, the amount of zinc deposited on steel should depend upon the concentration of zinc ions in the electrolyte. Actually, this is a way to control the zinc surface coverage. However, according to Chu *et al.* [19] a monolayer of UPD zinc is formed prior to bulk deposition and under such conditions the amount of deposited zinc does not depend upon the concentration of zinc ions in the solution. Bowles *et al.* [21] reported that UPD peaks of Bi on Pt have reached a more or less constant value when Bi content in the electrolyte changes from 1.205 to 4.22 μM. A similar behaviour was also observed by the same author [22] for copper UPD on Pt and by Adzic *et al.* [23] for lead UPD on Pt. The amount of charge of the deposited monolayer is determined by the area under the absorption peak. Assuming that the maximum coverage (one layer of closely packed zinc atoms on the electrode surface) requires a charge of $Q_{max} = 450\ \mu C\ cm^{-2}$ [24], the degree of coverage of zinc was estimated to be $\theta_{Zn} = 0.88$. Note that the calculation of the zinc coverage from voltammetry peaks is very approximate [6, 7, 24].

Linear sweep voltammetric curves were also obtained on Inconel 718 substrates using the same

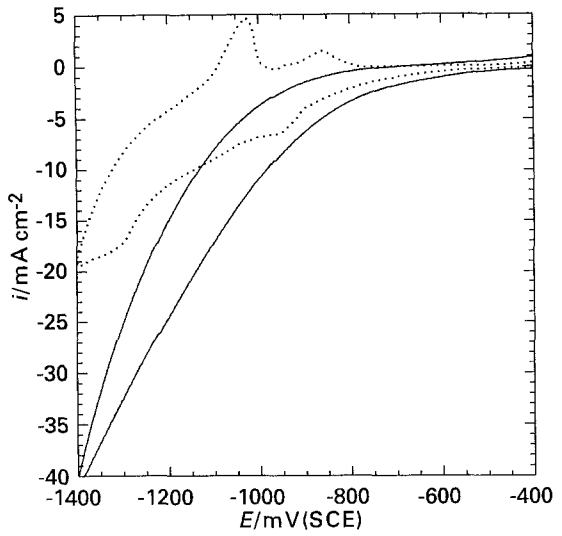

Fig. 3. Cyclic voltammetry curves obtained on Inconel 718 alloy by using the electrolyte containing 1 M Na_2SO_4, 0.4 M NaCl, 1 M H_3BO_4 in the absence and presence of 5×10^{-3} M of Zn^{2+}, and sweep rate 500 mV s^{-1}. Key: (——) without Zn^{2+}; (· · · · · ·) 5×10^{-3} M Zn^{2+}.

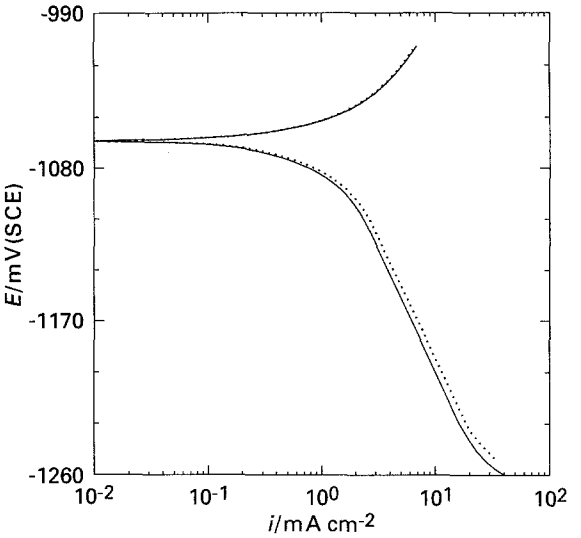

Fig. 4. Cathodic polarization curves recorded on AISI 4340 electrode and Inconel 718 electrode with bulk deposition of zinc. Predeposition potential −1100 mV vs SCE, predeposition time 5 min. Key: (——) bulk zinc on AISI 4340 substrate; (· · · · · ·) bulk zinc on Inconel 718 substrate.

supporting electrolyte and sweep rate of 500 mV s^{-1}. The corresponding curves obtained in the absence and presence of 5×10^{-3} M zinc ions are given in Fig. 3. When starting the cathodic sweep from −400 mV vs SCE, two well defined cathodic peaks at −950 mV vs SCE and at −1350 mV vs SCE are observed. The first peak occurs at potential which is more noble than the Nernst potential (−1070 mV vs SCE) and corresponds to underpotential deposition of zinc on Inconel 718 substrate. The second peak corresponds to the bulk deposition of zinc from the electrolyte. According to Fig. 3, a decreasing of the hydrogen evolution is observed when the experiments were carried out in the presence of 5×10^{-3} M of Zn^{2+}. On the anodic side two stripping peaks at −1030 mV vs SCE and at −860 mV vs SCE are observed and correspond to zinc dissolution and zinc disorption peak, respectively. The amount of charge of the deposited monolayer is determined by the area under the absorption peak. Assuming that the maximum coverage requires a charge of $Q_{max} = 450\,\mu C\,cm^{-2}$ [24], the degree of coverage of zinc on Inconel 718 substrate was estimated to be $\theta_{Zn} = 0.5$.

3.2. *Polarization measurements*

The polarization studies were carried out using electrodes with an area of 0.5 cm^2 in the absence and presence of Zn^{2+} (0.1 M of Zn^{2+} for AISI 4340 electrodes and 5×10^{-3} M of Zn^{2+} for Inconel 718 alloy electrodes) in an electrolyte containing 1 M Na_2SO_4, 0.4 M NaCl and 1 M H_3BO_3. The electrodes were held at different cathodic potentials for 5 min to ensure zinc deposition on the surface. As shown in Fig. 4, the bulk deposition of zinc on AISI 4340 and Inconel 718 substrates occurs at −1100 mV vs SCE in agreement with the results obtained using cyclic voltammetry. Potentials more positive than the Nernst equilibrium potential were applied to obtain various coverages of zinc on the substrate surfaces.

The cathodic polarization curves obtained for hydrogen evolution reaction on bare AISI 4340 steel from sulfate electrolytes and on AISI 4340 steel with potentiostatically predeposited zinc from the same supporting electrolyte in which 0.1 M Zn^{2+} ions were added are shown in Fig. 5. According to Fig. 5, the presence of zinc ions on the surface inhibited the hydrogen evolution reaction (HER). The hydrogen evolution current density in the presence of zinc ions is reduced from 77.4 to 44.6 $\mu A\,cm^{-2}$. The results obtained from the polarization studies are summarized in Fig. 6 in which the hydrogen evolution current $(i_a - i_P)/i_a\%$ at −700 mV vs SCE in the presence (i_P) and absence (i_a) of predeposited zinc is plotted as a function of the applied potentials. The HER is reduced by 46% compared with the

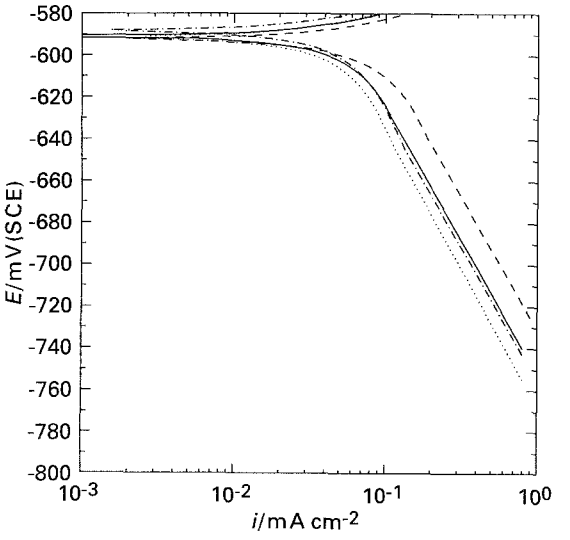

Fig. 5. Cathodic polarization curves obtained on AISI 4340 electrode by using electrolyte containing 1 M Na_2SO_4, 0.4 M NaCl, 1 M H_3BO_4 (pH 4) and on AISI 4340 electrode predeposited with zinc from the same electrolyte containing 0.1 M Zn^{2+}. Predeposition time 5 min and scan rate 1 mV s^{-1}. Key: (– – –) without predeposition; (——) E_{pdep}/mV vs SCE: (——) −720, (– · –) −770 and (· · · · · ·) −870.

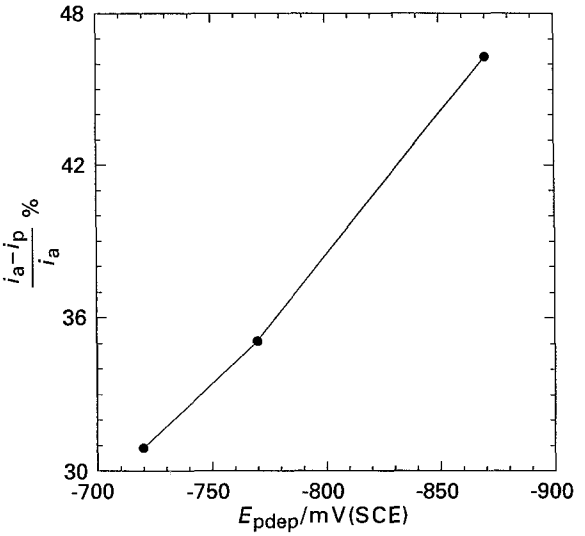

Fig. 6. Dependence of hydrogen evolution current on AISI 4340 electrode computed at −700 mV vs SCE from Fig. 5 as a function of the applied potential.

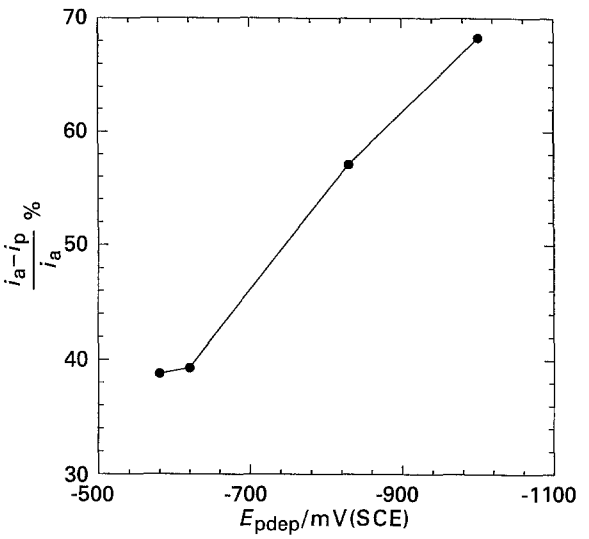

Fig. 8. Dependence of hydrogen evolution current on Inconel 718 electrode computed at −600 mV vs SCE from Fig. 7 as a function of the applied potential.

corresponding value obtained on a bare AISI 4340 steel surface.

In the absence of zinc, a linear region with a Tafel slope of 127 mV (decade)$^{-1}$ $\alpha_c = 0.46$ and $i_0 = 9.8 \times 10^{-3}$ μA cm^{-2} were obtained indicating activation control for HER in the potential region between −620 mV and −720 mV vs SCE. In the presence of zinc ions on the surface [at predeposition potential of −870 mV vs SCE], the Tafel slope is 132 mV (decade)$^{-1}$ with $i_0 = 7.9 \times 10^{-3}$ μA cm^{-2} and $\alpha_c = 0.44$.

The corresponding cathodic polarization curves obtained for hydrogen evolution reaction on Inconel 718 surface are given in Fig. 7. As seen in Fig. 7, the hydrogen evolution reaction is inhibited in the presence of underpotential deposited zinc. The inhibiting effect is shown in Fig. 8, where hydrogen evolution current at −600 mV vs SCE is plotted as a function of the predeposition potentials. According to Fig. 8, the HER current density on Inconel 718 alloy surface with deposited monolayer of zinc is reduced by 68% compared with the corresponding current obtained on a bare Inconel 718 surface.

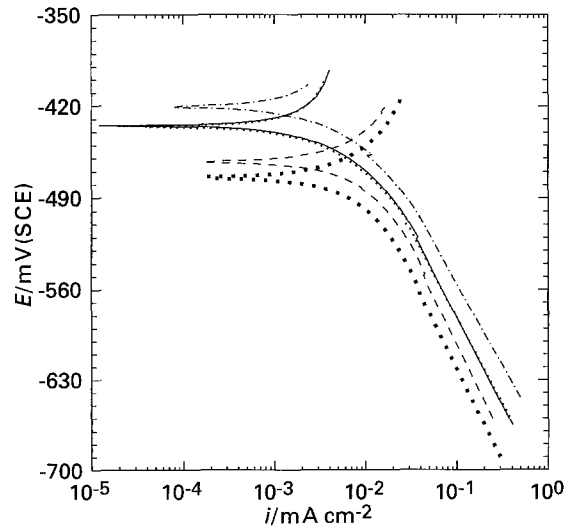

Fig. 7. Tafel curves obtained on Inconel 718 alloy with and without predeposition of zinc on the substrate. Predeposition time 5 min and scan rate 1 mV s^{-1}. Key: (– · –) without predeposition; E_{pdep}/mV vs SCE: (· · · · · ·) −580, (——) −620, (– – –) −830 and (■ ■ ■) −1000.

Two basic mechanisms have been accepted for hydrogen evolution. These are (i) the recombination mechanism, expressed as

$$H^+ + e^- + M \longrightarrow MH_{ads} \quad (4)$$

$$MH_{ads} + MH_{ads} \longrightarrow 2M + H_2 \quad (5)$$

where M signifies the substrate on which hydrogen evolution occurs, and (ii) the electrochemical desorption mechanism, expressed as

$$M + H^+ + e^- \longrightarrow MH_{ads} \quad (6)$$

$$MH_{ads} + H^+ + e^- \longrightarrow H_2 + M \quad (7)$$

According to Bockris *et al.* [25] and McBreen *et al.* [26], the hydrogen evolution reaction on an iron substrate in acidic electrolytes is determined by the coupled discharge-recombination mechanism. Assuming the Langmuir adsorption isotherm, Subramanyan *et al.* [1] have shown theoretically that the discharge–recombination mechanism is operative at low degree of surface coverage by atomic hydrogen. Thus one can expect that a partial monolayer of underpotential deposited zinc on the most active adsorption centres on the substrate will inhibit the hydrogen evolution reaction.

3.3. *Hydrogen permeation studies*

When carrying out experiments with a bipolar membrane, the steady state rate of hydrogen penetration in a diffusion mode can be presented by the following equations obtained for two typical boundary conditions: (i) in the case where the hydrogen concentration at the entry side of the membrane is constant (C condition) [27]:

$$\frac{j_t - j_0}{j_\infty - j_0} = 1 + 2\sum_{n=1}^{\infty}(-1)^n \exp(-n^2\pi^2\tau) \quad (8)$$

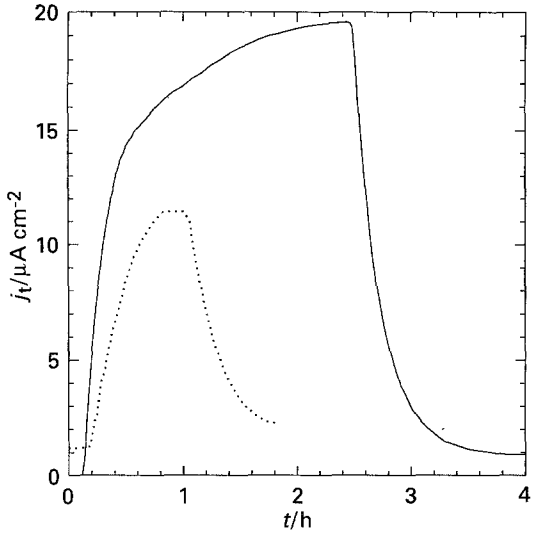

Fig. 9. Hydrogen permeation transients through AISI 4340 steel membrane obtained at $E_c = -1000\,mV$ vs SCE in the presence and absence of 0.1 M Zn^{2+} in an electrolyte containing 1 M Na_2SO_4, 0.4 M NaCl, 1 M H_3BO_3 (pH 4), and membrane thickness 0.45 mm. Key: (——) without Zn^{2+}; (·····) 0.1 M Zn^{2+}.

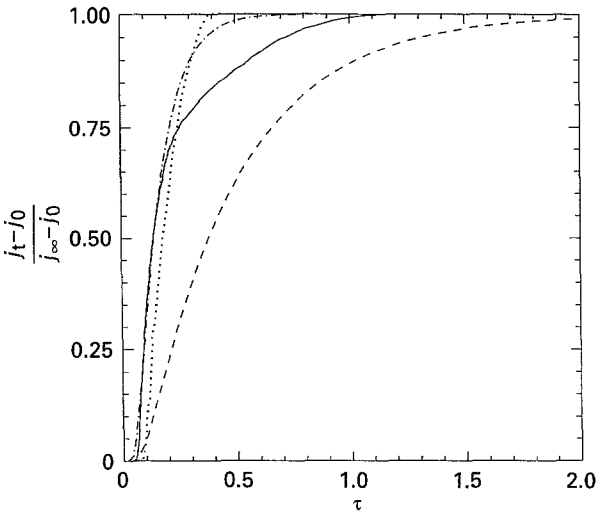

Fig. 11. Comparison of the dimensionless hydrogen permeation transients given in Fig. 9 with the two typical theoretical solutions given by Equations 8 and 9. Key: (——) without Zn^{2+}; (·····) 0.1 M Zn^{2+}; (–·–) constant concentration condition; (– – –) constant flux condition.

and (ii) in the case where the flux of the hydrogen entering the membrane is constant (F condition) [28]:

$$\frac{j_t - j_0}{j_\infty - j_0} = 1 - \frac{4}{\pi}\sum_{n=0}^{\infty}\frac{(-1)^n}{(2n+1)}\exp\left\{\frac{-(2n+1)^2\pi^2\tau}{4}\right\} \tag{9}$$

where j_t is transition hydrogen permeation current density, j_0 the initial hydrogen permeation current density (may or may not be zero), j_∞ the steady state hydrogen permeation current density, $\tau = tD/L^2$, where t is time, D is the hydrogen diffusivity and L is the membrane thickness. It is widely accepted in the literature, that when the hydrogen is generated at constant potential, at the entry side of the membrane C condition will be established, while in the case when the hydrogen is generated at constant current, the F condition will be established.

To investigate if any inhibition of the hydrogen permeation occurs in the presence of the underpotential deposited zinc, the hydrogen permeation through AISI 4340 steel (0.1 M Zn^{2+}) and through Inconel 718 (5×10^{-3} M Zn^{2+}) membranes with thicknesses of 0.45 mm and 50 μm, respectively was studied in a conventional zinc plating solution [1 M Na_2SO_4 + 0.4 M NaCl + 1 M H_3BO_3] at potential of −1000 mV vs SCE. According to our potentiodynamic studies, at this potential the underpotential deposition of zinc occurs from sulfate electrolytes. The resulting hydrogen permeation transients in the presence and absence of zinc through AISI 4340 steel is shown in Fig. 9. The same dependence for Inconel 718 is presented in Fig. 10. From hydrogen permeation transients obtained in the absence of zinc ions,

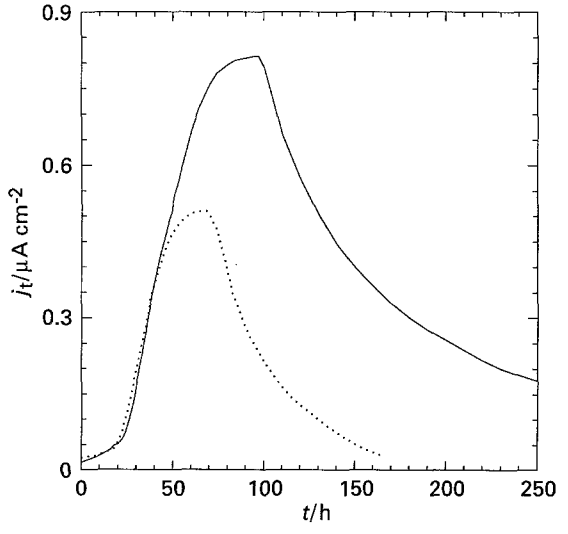

Fig. 10. Hydrogen permeation transients through Inconel 718 alloy membranes at $E_c = -1000\,mV$ vs SCE in the presence and absence of 5×10^{-3} M Zn^{2+} in the electrolyte, and membrane thickness 50 μm. Key: (——) without Zn^{2+}; (·····) 5×10^{-3} M Zn^{2+}.

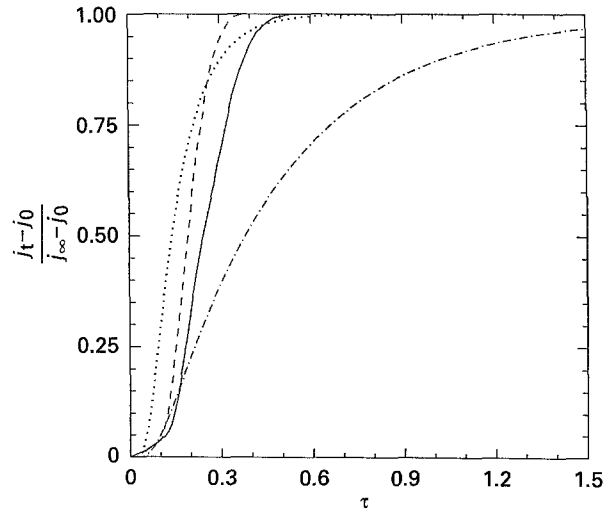

Fig. 12. Comparison of the dimensionless hydrogen permeation transients given in Fig. 10 with the two typical theoretical solutions according to Equations 8 and 9. Key: (——) without Zn^{2+}; (– – –) 5×10^{-3} M Zn^{2+}; (·····) constant concentration condition; (–·–) constant flux condition.

the hydrogen diffusion coefficient through AISI 4340 steel and Inconel 718 alloy was calculated to be $2.6 \times 10^{-7}\,cm^2\,s^{-1}$ and $3.2 \times 10^{-11}\,cm^2\,s^{-1}$, respectively. Similar results for the hydrogen diffusivity through AISI 4340 steel and Fe-Ni alloys were obtained in the literature [29, 30].

The dimensionless hydrogen permeation current density vs the dimensionless time are presented and compared with the theoretical solutions of Equations 8 and 9 in Fig. 11 and Fig. 12. According to these figures, the hydrogen permeation transients through AISI 4340 and Inconel 718 are approaching C condition solution using P method.

4. Conclusion

The polarization experiments show that deposited zinc effectively inhibits the discharge of hydrogen up to 46% and 70% compared with the currents obtained on the bare AISI 4340 steel and Inconel 718 alloy, respectively. In the presence of monolayer coverage of zinc on the substrate, the hydrogen permeation rate through AISI 4340 steel and Inconel 718 alloy membrane is reduced by 51% and 40%, respectively. The observed inhibition effect is due to an underpotential deposition of zinc on the alloy substrate, which changes the chemical properties of the substrate and reduces the surface coverage of hydrogen.

Acknowledgement

Technical assistance and financial support by A. John Sedriks, the Office of Naval Research, under contract no. N00014-92-J-1434 are gratefully acknowledged.

References

[1] P. Subramanyan, *in* 'Comprehensive Treatise of Electrochemistry', (edited by J. O'M Bockris, Brian E. Conway, Ernest Yeager and Ralph E. White), Plenum Press, New York (1981) 4, p. 411.
[2] S. Bagaev, K. Pedan and V. Kudryavtsev, *Zatshtita Metallov* **19** (1983) 968.
[3] V. Kudryavtsev, K. Pedan, H. Barbashkina and S. Vagramjan, *ibid* **9** (1973) 161.
[4] J. J. Reilly, *Z. Phys. Chem.* **117** (1979) 655.
[5] R. N. Iyer, H. W. Pickering and M. Zamanzedeh, *J. Electrochem. Soc.* **136** (1989) 2463.
[6] D. M. Kolb, *in* 'Advances in Electrochemistry and Electrochemical Engineering', (edited by H. Gerischer and, C. W. Tobias), John Wiley & Sons, New York (1978) 11, p. 125.
[7] R. R. Adzic, *in* 'Advances in Electrochemistry and Electrochemical Engineering', (edited by H. Gerischer, and C. W. Tobias), John Wiley & Sons, New York, (1982) 13, p. 159.
[8] D. M. Kolb, M. Przasnyski and H. Gerischer, *J. Electroanal. Chem.* **54** (1974) 25.
[9] D. M. Drazic and L. Z. Vorkapic, *Corros. Sci.* **18** (1978) 907.
[10] A. Despic and M. Pavlovic, *Electrochim. Acta* **27** (1982) 1539.
[11] S. Rashkov, C. Bozhkov, V. Kudryavtsev, K. Pedan and S. Bagaev, *J. Electroanal. Chem.* **248** (1988) 421.
[12] G. Zheng, B. N. Popov and R. E. White, *J. Electrochem. Soc.* **140** (1993) 3153.
[13] G. Zheng, B. N. Popov and R. E. White, *ibid* **141** (1994) 1220.
[14] B. N. Popov, G. Zheng and R. E. White. To be published in *Corrosion*, August, (1994).
[15] G. Zheng, B. N. Popov and R. E. White, *J. Electrochem. Soc.* **141** (1994) 1526.
[16] B. N. Popov, G. Zheng and R. E. White. To be published in *Corros. Sci* (1994).
[17] M. A. V. Devanathan and L. Stachurski, *Proc. R. Soc. Lond.* **A270** (1962) 90.
[18] S. Trasatti, *J. Electroanal. Chem.* **33** (1971) 351.
[19] G. Adzic, J. McBreen and M. G. Chu, *J. Electrochem. Soc.* **128** (1981) 1691.
[20] M. G. Chu, J. McBreen and G. Adzic, *ibid* **128** (1981) 2281.
[21] B. J. Bowles, *Electrochim. Acta* **15** (1970) 737.
[22] B. J. Bowles, *ibid* **15** (1970) 789.
[23] R. R. Adzic, M. D. Spasojevic and A. R. Despic, *ibid* **24** (1979) 569.
[24] A. Frumkin, *in* 'Advances in Electrochemistry and Electrochemical Engineering', (edited by P. Delahay and C. W. Tobias), Interscience, New York (1963) 3, p. 163.
[25] J. O'M. Bockris, J. McBreen and L. Nanis, *J. Electrochem. Soc.* **112** (1965) 1027.
[26] J. McBreen and A. M. Genshow, Proceedings of the Conference on Fundamental Aspects of Stress Corrosion Cracking, NACE Columbus (1969) p. 51.
[27] M. A. V. Devanathan, Tech. Rep. ONR/551/22/NR-036-028, Office of Naval Research (1961).
[28] N. Boes and H. Zuchner, *J. Less-Common Metals* **49** (1976) 223.
[29] W. Beck, J. O'M Bockris, J. M. Breen and L. Nanis, *Proc. R. Soc. Lond.* **A290** (1966) 220.
[30] W. M. Robertson, *Metall. Trans.* **10A** (1979) 489.